

# The Role of HF Ocean Surface Radar in Australia as a Long-term Coastal Ocean Monitoring Facility

Mal L. Heron

School of Mathematical and Physical Sciences, James Cook University, Townsville, QLD

## Abstract

HF ocean surface radar technology has now developed to a point where permanently installed monitoring systems are being used for planning and operational purposes in several countries. In Australia and New Zealand there have been research and development systems but, apart from the defence sector, there have been no installations for monitoring for commercial benefit or long-term research projects. This is now changing. HF radar systems are now available commercially. The technology has a proven reliability in the mapping of surface currents, and is showing good results for wave and wind parameters. There are three conceptual approaches to HF radar systems which are quite fundamentally different and each of which will give best results under certain constraints and commercial needs. The three approaches are all available commercially. This paper reviews the HF ocean radar concept and outlines the benefits of each approach. We also map out a plan for the way in which this technology might develop in Australia. There are obvious beneficiaries in having local monitoring systems; for those in coastal engineering, management and leisure activities. There are also benefits in providing quality data in near real time to data networks like that run by the Bureau of Meteorology, and the Australian node of the Global Ocean Observing System: OZGOOS.

## 1 Introduction

The underlying physics of HF radar was discovered by Crombie (1955) as interfering clutter on an ionospheric sounder. Crombie found a characteristic structure in the spectrum of the sea echoes by observing two strong frequency-shifted echo lines a fraction of 1 Hz above and below the transmitted wave frequency. For a single antenna, the echo spectrum would look like the stylised diagram in Fig. 1 for a given range gate, set by opening the receiver for an interval  $\Delta t$  seconds following a delay of  $t$  seconds after each radiated pulse from the radar transmitter. Fig. 2 shows the ranging configuration, and with an omni-directional antenna echo energy would come from the annular band at the range specified by  $r = ct/2$  where  $c$  is the electromagnetic phase speed.

In each radar look direction,  $\theta$ , shown in Fig. 2 there is a resonant Bragg echo in the backscatter direction from waves propagating along the radial and having wavelength  $\lambda_s$  which is half the radar wavelength,  $\lambda_0$ . There are two sea surface waves which satisfy this Bragg condition. One has wavelength  $\lambda_s$  and is propagating in the direction of  $\mathbf{r}$ , and the other has the same wavelength propagating in the direction  $-\mathbf{r}$ . The sea surface gravity wave with wavelength  $\lambda_s$  has phase celerity  $c_s = \sqrt{g\lambda_s/2\pi}$ , if we adopt the deep water approximation. The Doppler shift imposed on the radio wave when it scatters from the sea surface wave is then

$$f_0 = \pm \sqrt{\frac{g}{2\pi\lambda_s}}, \quad (1)$$

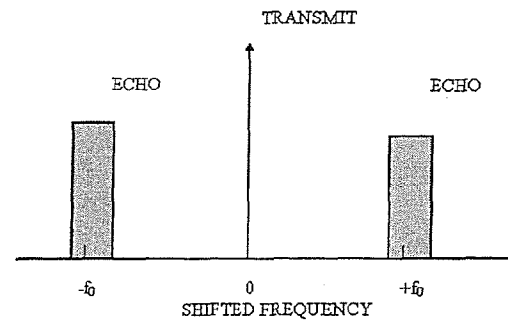


Figure 1 Stylised ocean echo spectrum using an omnidirectional antenna.

and these are the  $f_0$  annotations shown on Fig. 1. Note that this is the same Doppler shift for all radar look angles,  $\theta$ , because the Bragg condition is invariant with  $\theta$  when there is no current. The amplitude of the signal may vary with  $\theta$  because there is usually a variation of sea wave amplitudes as the look direction varies about the direction of the wind. For an omnidirectional antenna these amplitudes superpose for all possible angles,  $\theta$ , at the range  $r$ .

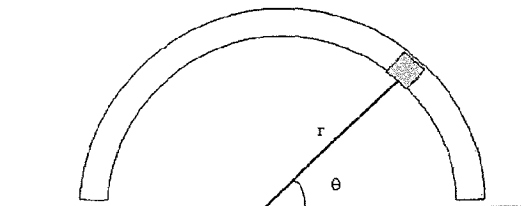


Figure 2 Radar geometry: for an omnidirectional antenna and conventional time-gate for range, the ocean echo will come from the range of angles,  $\theta$ , but from only one range,  $r$ .

So, what causes the spreading of the echo energy about  $\pm f_0$  in Fig. 1?

If there is a surface current flowing across the radar coverage area then there is an additional Doppler shift on the echoes. For any given radar look angle,  $\theta$ , a surface current with a component  $v_r$  in the radial direction will by simple superposition, produce a Doppler shift of  $f_0 + \Delta f$  given by

$$f_0 + \Delta f = \pm \sqrt{\frac{g}{2\pi\lambda_s} - \frac{2v_r}{\lambda_s}} \quad (2)$$

The assumption of superposition is acceptable as long as the surface current velocity is not close to the phase velocity of the Bragg wave. With reference to Fig. 1, this means that the broadening of the peak should not be close to the Doppler shift frequency,  $f_0$  caused by the phase speed of the Bragg wave.

Now, however, the projection of the surface current onto the radial does depend on the angle,  $\theta$ , so from the one arc at range  $r$ , shown in Fig. 2, we get a spread of Doppler shifts about the  $f_0$  value. It is this band of frequency shifts, which arise from the surface current, that we show in Fig. 1. In practice the frequency resolution within the Doppler shift frequency band can be very good. For example, if the radar samples for 100 s, the frequency resolution in the spectrum is 0.01 Hz. The Bragg Doppler frequency is typically 0.3-0.5 Hz and the Doppler shift due to surface current is typically in the range  $\pm 0.2$  Hz.

The variation between different types of HF radars comes down to the way in which they deduce the direction,  $\theta$ , which corresponds to each frequency in the spread peak shown in Fig. 1.

Once the frequency shift and the direction are determined, we can extract the radial component of velocity for grid points over the area. It is necessary with all HF radar systems to have a second radar station sampling the same grid point from an angle preferably about  $90^\circ$  away. Then the surface current vector can be re-constructed.

## 2 Direction-finding based on amplitude

The amplitude method uses a combination of antenna beam patterns to deduce the angle,  $\theta$ , for each frequency component in the Doppler spread spectrum. The SEASONDE system uses two vertical loop antennas and a vertical whip, for which the antenna patterns are shown in Fig. 3.

If the antenna patterns are known, and the amplitude measured for each frequency component on each of

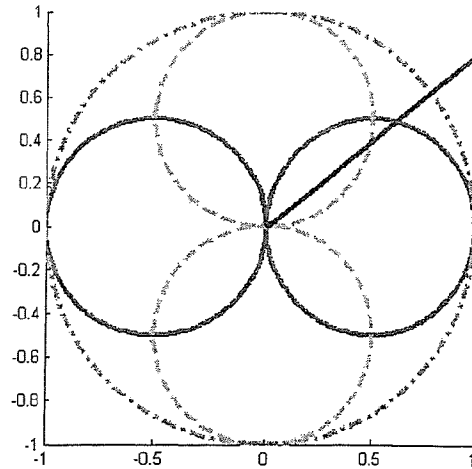


Figure 3 Antenna patterns for the crossed loops and vertical whip antennas. The solid and dashed lines are for the vertical loop antennas and the dot-dash line is for the omni-directional whip used for calibration. The straight line in the first quadrant indicates an incoming signal.

the loops, then the direction of the incoming signal can be derived. If a specific Doppler shift frequency is produced at more than one position on the target arc, then this simple analysis does not work.

The analysis algorithm is improved by using a direction finding algorithm called Multiple Signal Classification (MUSIC) (Schmidt, 1986) to sort out multiple point sources. Barrick and Lipa (1997) evaluate the accuracy of the MUSIC algorithm using simulated data where they also discuss a five-element antenna which gives improved resolution of multiple point sources of the same frequency.

The main advantage of the crossed loop direction-finding HF radar system is its small footprint antenna. This antenna sits on a single pole with a transmitter on another pole nearby. This radar station can be set up in places where other, larger antennas, could not be used. The amplitude DF system is an important option for the HF community because of the flexibility that the small antenna offers. There are some performance trade-offs with the amplitude system. The technique is sensitive to antenna polar patterns, and especially to any changes. The presence of metal objects within a couple of wavelengths of the antenna (including in the ground) can affect the antenna patterns. These can be calibrated and the set-up procedure includes the determination of the actual (rather than theoretical) patterns which are then used in the analysis. The system remains sensitive to subsequent changes in the patterns. Some users have experienced quite long settling-in periods to gain experience in the site calibration.

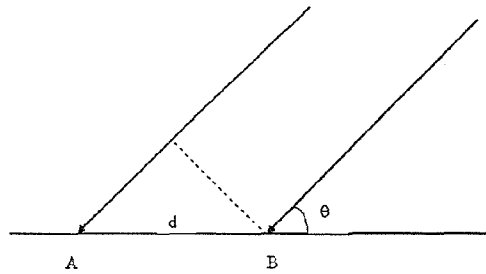


Figure 4 Schematic of signals from a point source impinging on a two-antenna receiver array. The two antennas are separated by distance  $d$ , which would normally be  $\frac{1}{4}$  to  $\frac{1}{2}$  wavelength.

### 3 Direction-finding based on phase

In principle, two antennas spaced about one-quarter to a half wavelength apart can detect the direction of arrival of a signal from a point source. Consider a close-up of the radar site in Fig. 2, where the signal is arriving from angle  $\theta$  as shown in Fig. 4. The phase difference between the signals received at the two antennas is given by

$$\Delta\phi = 2\pi d \cos\theta / \lambda \quad (3)$$

where  $\lambda$  is the radar wavelength. If we measure  $\Delta\phi$  we can find the angle  $\theta$ .

The analysis follows the same path as for the Amplitude Direction-Finding method. The phase and amplitude is recorded at each antenna as a time series over a period of, say, 100 seconds and an FFT carried out to produce a Doppler Shift Spectrum like that shown in Fig. 1. Then for each frequency component of the spread peak, we use the phase relation to determine the direction. For two antennas we can analyse only one direction; for  $N$  antennas it is possible, in closed form, to determine  $N-1$  signal directions which might contribute to that Doppler Shift frequency. Common practice has indicated that four antennas arranged in a square whose side is  $\lambda/4$  is a satisfactory trade-off for most coastal ocean surface current patterns (Barrick et al., 1977;

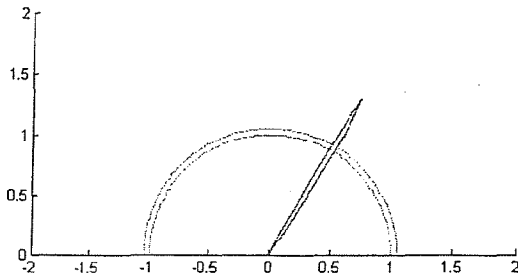


Figure 5 Schematic showing the beam formed by a 16-element array spaced at  $\lambda/2$  and a range-gated annular target area.

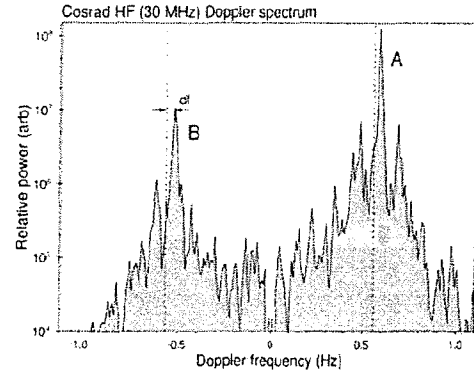


Figure 6 A typical Doppler Shift spectrum from a beam-forming radar receiver. The JCU 30 MHz COSRAD system.

Gurgel, 1997). The MUSIC algorithm can be used to do the analysis for multiple direction signals.

The advantages of the direction-finding by phase measurements is that phase is more precise than amplitude measurement, and the measurement is more robust.

### 4 Beam-forming

The optimum spacing for a phased array to form the narrowest beam with the lowest sidelobes is  $\lambda/2$ . This configuration is illustrated in Fig. 5. As the beam is steered (by relative phase shifts to the antennas) the beam broadens until it is unusable when parallel to the coast. In practice the beam is generally operated within  $\pm 45^\circ$  of the normal to the array line. In this system the small target area is completely specified by the range-gating and by the beam. The Doppler Shift on the signal from that single direction is unique and a sharp first-order line is observed, rather than the broadened band illustrated in Fig. 1.

A typical spectrum from a beam-forming radar is shown in Fig. 6 where the two Bragg peaks are labelled A and B, and the Doppler Shift due solely to the Bragg waves is indicated by dashed lines. The Doppler Shift offset due to surface current in that pixel is labelled as  $df$  and the vertical dashed lines indicate the theoretical deep-water position of the first-order Bragg lines.

The unambiguous location of the pixel on the ocean surface and the observed Doppler shift spectrum from a single point source make this approach more robust than the alternatives. Surface currents can be extracted from spectra with lower signal-to-noise ratios, which means that for similar radar power and modulation type, the beam-forming system will operate to longer ranges. An advantage of the beam-forming spectrum shown in Fig. 6, is that the second-order energy in the spectrum (which is over

20 db above the noise) can be used to derive wave height parameters.

The main disadvantage of the beam-forming approach is in the site requirements. For a radar operating at 25 MHz with a 16-element receive array, an area of about 100m alongshore and 5m deep must be found. The WERA radar is technically superior because of its low system noise. It has options of 8, 12 or 16 elements in the phased array of antenna elements.

## 5 Currently available remote sensing parameters

### 5.1 Surface currents

The parameter that has attracted most interest in HF ocean surface radar is the sea surface current map. This is available from all versions and the map can be updated with a new set of observations on the order of one hour. It is not surprising that this emerges as the primary product from HF radar because it offers an enormous improvement on any other way to measure currents in coastal waters. In all systems two radar sites are required to extract surface current velocity vectors because a single station can determine only the radial current. An example of a surface current map is shown in Fig. 7 using the beam-forming COSRAD system in the lower end of Port Phillip Bay in Victoria, Australia.

The surface current product has been quite thoroughly evaluated and compared with in situ methods of moored meters and acoustic sounders (Graber et al., 1997). This is a mature product and it is increasingly likely that management and development agencies will accept the product without proof of concept against the alternatives. An application of the usefulness of successive hourly maps of surface current is shown in Fig. 8.

These are near-Lagrangian tracks of notional parcels of surface water. The surface velocity vector is found by interpolation on a map at the starting

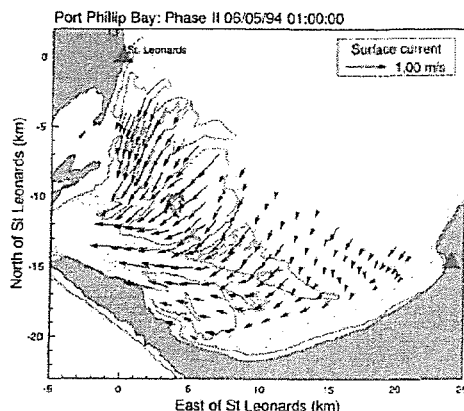


Figure 7 Surface currents in the Great Sands Region of Port Phillip Bay at Ebb Tide, measured by JCU's COSRAD beam-forming HF radar.

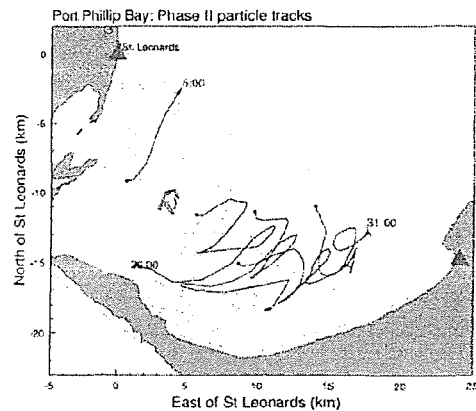


Figure 8 Computed tracks taken from the starting dot and using successive hourly maps of surface currents like that shown in Fig. 7. When a track runs off the mapped area the number indicates the time that it was observed. Particle tracks is a routine product from HF sea surface radars. It has application in search-and-rescue, and in reef connectivity studies.

time, and the parcel is moved at that velocity for one time step (usually 1 hour). Then, on the next map, one time step later the velocity is determined at the new location, and so on. The parcel tracks can be drawn from any starting point on the mapped area, or starting time. The applications for oil spill management and search-and-rescue operations are obvious.

### 5.2 Wind direction

Observations of wind direction over the area of mapping are available from all systems and arise from consideration of the relative energy in the first-order peaks (labelled A and B in Fig. 6). The analysis requires the adoption of a wave directional spreading model. In addition there is an ambiguity for a single station because it is not possible to differentiate between two possible wind directions symmetrically placed about the radar look direction (however that is determined). If one assumes that a system consists of two radar sites in order to produce surface current maps, then at each point on the sea surface there are two determinations of first-order ratio and, theoretically (with no noise) there is a closed solution for the dominant direction of the Bragg waves. For waves with wavelength 10-20m this represents the wind direction except only in conditions of rapid wind shifts, when a settling time of about half an hour has to be considered (Heron and Prytz, 2002).

People are having reasonable success with the determination of wind direction from dual radar systems, although from an operational point of view there is still a need to validate the product in the local setting.

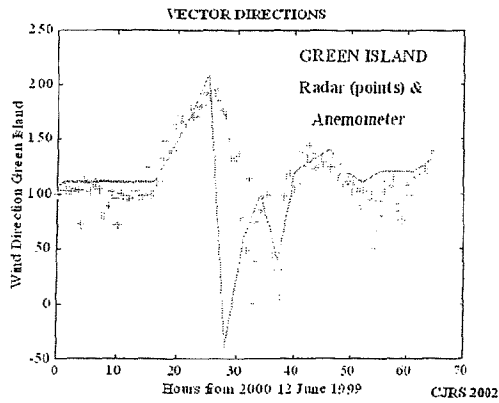


Figure 9 COSRAD wind directions (+) compared with anemometer wind directions (line) around Green Island. During the observation period a weak meteorological front came across the region and the wind rotated through 360 degrees. The radar determination exhibits a delay while the sea waves are re-established in the new direction. We think the offset in direction is due to a local effect on the anemometer. (After Heron et al., 2002)

An example of the determination of wind direction is shown in Fig. 9. These data were obtained from the beam-forming COSRAD HF radar for pixels within a 5 km radius of Green Island in the northern section of the Great Barrier Reef. The validation data came from an anemometer on the island.

### 5.3 Significant wave heights

A weighted integral of the second-order energy surrounding the Doppler lines in Fig. 6 is determined by the root-mean-square (RMS) wave height on the sea surface (Barrick, 1977). This algorithm has two main limitations. It does not apply when the radar look direction is near orthogonal to the wind direction, and there is a saturation limit for rms wave heights above which higher order energy becomes significant and the algorithm does not work. This limit is determined by the radar wavenumber  $k_0$  in the relation

$$h_{s,max} = \frac{2}{k_0}. \quad (4)$$

For a 25 MHz radar this limit is at about 4m. Dual station systems solve the orthogonality restriction.

There has been reasonable success with this product, spurred on by the need for operational data for the large aluminium catamaran ferries - where the operational limit is near 4m rms (Maresca and Georges, 1980; Heron and Heron, 1998; Wyatt, 1988). It is likely that any rms waveheight product will still need validation by point in situ measurements in applications work over the next few years.

Significant wave height mapping can be done only with beam-forming radar systems. Recent work is

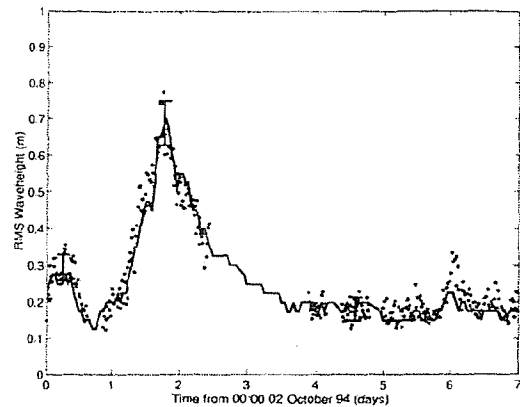


Figure 10 Significant wave heights extracted from the beam-forming OSCAR HF radar at Duck, North Carolina. The radar data from pixels within 5 km of a wave buoy are shown as dots, and the buoy data are represented by the line. (After Heron and Heron, 1988)

showing that rms wave heights in water close to the site can be obtained from direction-finding radars (Lipa and Barrick, 2004). This analysis assumes that the directional spread can be determined in the first pixel from the radar.

### 5.4 Wave directional spectrum

Several researchers are working on the production of full directional wave spectra from the second-order spectrum obtained from dual beam-forming radar systems. While there have been some impressive results comparing radar-derived spectra with those from wave buoys, the directional wave spectrum product will probably require validation at specific sites in applications work (Wyatt, 1990; Howell and Walsh, 1993; Hisaki, 1996; Hashimoto et al., 2003).

Directional spectrum products are available only from beam-forming dual station systems, and then only when there is a very good signal-to-noise ratio.

### 5.5 Routine detection of swell parameters

An algorithm has been developed (Bathgate et al., 2005; these proceedings) to extract swell parameters on a routine basis. Their approach circumvents the complexities of a full wave directional spectrum analysis by adopting a simplified, but approximate, modulation theory approach to the swell component in the radar Doppler spectrum. This work shows the promise of being a routine real-time analysis to extract swell period, direction and height.

### 6. Range of the radars

The maximum range of operation is determined mainly by the operating frequency. For the same frequency and power, the phased array systems generally work to a higher range. Table 1 gives indicative ranges for the different frequency bands for all types of systems. Pixel size for the range dimension is governed by timing and there fore is

controlled by radar bandwidth. Normally it is difficult to find clear bands at lower frequencies, so in practice, there is an approximate relationship between frequency and range resolution. This is also indicated in Table 1.

Table 1  
Relationships between operating frequency, maximum operating range and range resolution.

Frequency Band (MHz)	Approx max range (km)	Approx pixel size (km)
6-10	150-200	5-7
10-20	100-150	3-5
20-30	60-100	2-4
30-60	10-50	0.3-2
60-180	3-10	0.08-0.30

These are indicative values and any of the suppliers of these systems will tailor a system to a specific application.

## 7 Current developments

### 7.1 Bistatic Systems

With the rapid increase in the number of HF radar systems being deployed around the world, for surface current mapping there is a developmental push towards bistatic radar systems. This is where one site transmits and another receives the sea echoes. The analysis for surface currents then requires some elementary trigonometry and the component of surface current for any given transmit and receive pair is in the direction of the bisector of the angles subtended by the stations to the pixel on the sea surface.

Bistatic systems generally use GPS timing for synchronization. The advantage of bistatic systems is that there is potential to reduce cost (one transmitter instead of two), especially where networks of radars are being considered along an extended coastline.

### 7.2 Assimilation of Surface Current Data into Predictive Models

Emphasis is turning away from the technology of the systems towards applications products, and a significant one amongst these is in the use of HF radar sea surface current in real-time (or near real-time) for now-casting and short-term forecasting. The potential for community use of these real-time products is significant as demonstrated by the work of New Jersey and in Monterey Bay. Work on alternative approaches to the numerical solution of Navier-Stokes' Equation is showing promise, where current maps are represented by dominant modes at a given location.

Delivery of radar products for real-time use by commercial and leisure communities is a significant task for the next phase of HF radar development.

## 8 Acknowledgements

The motivation for this review is the funding by the Australian Research Council (LE0560892) to install a monitoring HF ocean radar over the Capricorn/Bunker Reefs of the Great Barrier Reef. The main partner institutions for this venture are James Cook University, The University of Queensland, The Australian Institute of Marine Science, and the National Oceanic and Atmospheric Administration, USA. This installation is being done during 2005.

## 9 References

- Barrick, D.E., Extraction of wave parameters from measured HF sea echo Doppler spectra, *Radio Sci.*, *12*, 415-424, 1977.
- Barrick, D.E., M.W. Evans and B.L. Weber, Ocean surface currents mapped by radar, *Science*, *198*, 138-144, 1977.
- Barrick, D.E. and B. Lipa, Evolution of bearing determination in HF current mapping radars, *Oceanography*, *10*, 72-75, 1997.
- Graber, H.C, B.K. Haus, L.K. Shay and R.D. Chapman, HF radar comparisons with moored estimates of current speed and direction: Expected differences and implications, *J. Geophys. Res.*, *102*, 18,749-18,766, 1997
- Gurgel, K-W., Experience with shipborne measurements of surface current fields by radar, *Oceanography*, *10*, 82-84, 1997.
- Hashimoto, N., L.R. Wyatt and S. Kojima, Verification of a Bayesian method for estimating directional spectra from HF radar surface backscatter, *Coastal Engineering Journal*, *45*, 255-274, 2003.
- Heron, M.L. and A. Prytz, Wave height and wind direction from HF coastal ocean surface radar, *Canadian J. Remote Sensing*, *28*, 385-393, 2002.
- Heron, S.F. and M.L. Heron, A comparison of algorithms for extracting significant wave height from HF radar ocean backscatter spectra. *J. Atmos. Oceanic Tech.*, *15*, 1157-1163, 1998.
- Hisaki, Y., Nonlinear inversion of the integral equation to estimate ocean wave spectra from HF radar, *Radio Sci.*, *31*, 25-39, 1996.
- Howell, R. and J. Walsh, Measurement of ocean wave spectra using narrow-beam HF radar, *IEEE J. Oceanic Eng.*, *OE-18*, 296-305, 1993.
- Lipa, B. and B. Nyden, Directional wave information from the SeaSonde, *IEEE J. Oceanic Eng.*, in press, 2004
- Maresca, J.W., Jr. and T.M. Georges, Measuring rms wave height and the scalar ocean wave spectrum with HF skywave radar, *J. Geophys. Res.*, *85*, 2759-2771, 1980.
- Schmidt, R.O., Multiple emitter location and parameter estimation, *IEEE Trans. Antennas and Propagation.*, *AP-34*, 276-280, 1986.
- Wyatt, L.R. Significant waveheight measurement with HF radar, *Int. J. Remote Sensing*, *9*, 1087-1095, 1988.